

Brownian microhydrodynamics of active filaments

Abhrajit Laskar* and R. Adhikari†

The Institute of Mathematical Sciences, CIT Campus, Chennai 600113, India

Slender bodies capable of spontaneous motion in the absence of external actuation in an otherwise quiescent fluid are common in biological, physical and technological contexts. The interplay between the spontaneous fluid flow, Brownian motion, and the elasticity of the body presents a challenging fluid-structure interaction problem. Here, we model this problem by approximating the slender body as an elastic filament that can impose non-equilibrium velocities or stresses at the fluid-structure interface. We derive equations of motion for such an active filament by enforcing momentum conservation in the fluid-structure interaction and assuming slow viscous flow in the fluid. The fluid-structure interaction is obtained, to any desired degree of accuracy, through the solution of an integral equation. A simplified form of the equations of motion, that allows for efficient numerical solutions, is obtained by applying the Kirkwood-Riseman superposition approximation to the integral equation. We use this form of the equation of motion to study dynamical steady states in free and hinged minimally active filaments. Our model provides the foundation to study collective phenomena in momentum-conserving, Brownian, active filament suspensions.

I. INTRODUCTION

Slender bodies capable of spontaneous motion in viscous fluids are common in biological, chemical, physical and technological contexts. Examples from biology, in increasing degree of molecular complexity, include microtubules driven by molecular motors, axonemes, cilia, flagella [1–12], their synchronization and metachronal wave [13, 14]. In chemistry and physics, self-assembled bundles of microtubules driven by kinesin motors yields a model experimental system in which broken symmetry, collective excitations, and topological defects can be studied out of equilibrium [1, 2]. In technology, much recent research has been directed towards the synthesis of slender bodies capable of spontaneous motion [15–17]. Such self-actuated slender bodies are expected to have many microfluidic and biomimetic applications [18].

Despite the great variety in both the structure of the body and its mechanism of self-actuation, the examples above have three features in common: the spontaneous motion of the slender body produces flow in the ambient fluid, the body is of a size sufficiently small to make Brownian fluctuations important, and the body resists deformation produced by the spontaneous flow and Brownian fluctuations. Any universal emergent behaviour in active slender bodies must appear from the interplay between fluid flow, Brownian fluctuations and the elasticity. Such systems present a new class of fluid-structure interaction problems.

In this paper, we construct a theory of active slender bodies, by modeling them as filaments that enforce slip velocities or non-equilibrium stresses at the fluid-structure boundary. A multitude of microscopic mechanisms can produce such velocities or stresses. Our theory isolates the specific microscopic details of self-actuation

in the boundary conditions, from which universal, macroscopic fluid flow can be generated. Such flow results from the exchange of momentum between the body and the fluid, and since no external forces act on the body or the fluid, the sum of their linear momenta is conserved. In the absence of external torques, the sum of their angular momenta is similarly conserved. These two constraints are explicitly taken into account when computing the fluid flow within our theory.

The flow is computed through a discretization which replaces the continuous filament by a chain of spheres connected by non-linear springs. The spheres produce spontaneous hydrodynamic flow while the springs penalize changes in filament length and filament curvature. The antecedent of such a bead-spring discretization of a continuous filament traces back to Kramers, who used it to model the dynamics of a polymer. The crucial difference between the model of Kramers and our adaptation of it is that the spheres in our theory produce spontaneous flows. Each sphere must, therefore, be active. Such chains of active spheres have been used previously to model active filaments. In the earliest such model [19, 20], the spheres produce dipolar stresslet flows but are individually non-motile and are assumed so large that Brownian effects are negligible. In a subsequent contribution [21], the spheres are taken to be motile, Brownian effects are included in two-dimensions, but contributions from non-local hydrodynamic flow are neglected. In a related model, passive spheres are driven by tangential active stresses, hydrodynamically correlated Brownian motion is included in three-dimensions, but active flow is neglected [22, 23]. Our theory presented here contains all previous models as special cases.

In our recent work [24], the problem of computing the fluid flow of N active bodies has been solved by transforming the local conservation law for momentum, which under the conditions relevant to the microhydrodynamic regime is the Stokes equation, into an integral equation over the sphere boundaries. The solution of this boundary integral equation gives the rigid body motion of the

* abhra@imsc.res.in

† rjoy@imsc.res.in

active spheres, constrained by the conservation of linear and angular momentum, as a linear function of the forces, torques and the active boundary condition:

$$\mathbf{V}_n = \sum_{m=1}^N [\boldsymbol{\mu}_{nm}^{TT} \cdot \mathbf{F}_m^e + \boldsymbol{\mu}_{nm}^{TR} \cdot \mathbf{T}_m^e] + \sum_{m \neq n}^N \sum_{l=1}^{\infty} \left[\boldsymbol{\pi}_{nm}^{(T, l+1)} \odot \mathbf{V}_m^{(l+1)} \right] + \mathbf{V}_n^a, \quad (1a)$$

$$\boldsymbol{\Omega}_n = \sum_{m=1}^N [\boldsymbol{\mu}_{nm}^{RT} \cdot \mathbf{F}_m^e + \boldsymbol{\mu}_{nm}^{RR} \cdot \mathbf{T}_m^e] + \sum_{m \neq n}^N \sum_{l=1}^{\infty} \left[\boldsymbol{\pi}_{nm}^{(R, l+1)} \odot \mathbf{V}_m^{(l+1)} \right] + \boldsymbol{\Omega}_n^a. \quad (1b)$$

In the above, \mathbf{V}_n and $\boldsymbol{\Omega}_n$ are the velocity and angular velocity of the n -th particle, \mathbf{V}_n^a and $\boldsymbol{\Omega}_n^a$ are the self-propulsion and self-rotation contributions to the rigid body motion, the $\boldsymbol{\mu}$ are the usual mobility matrices that relate external forces and torques to the rigid body motion and the $\boldsymbol{\pi}$ are propulsion matrices [24] that relate $\mathbf{V}_m^{(l+1)}$, the l -th mode of the non-equilibrium slip velocity on the surface of the m -th particle, to the rigid body motion (see below). These relations clearly show that rigid body motion of active particles is possible in the absence of external forces and torques, $\mathbf{F}_m^e = 0$, $\mathbf{T}_m^e = 0$, and even in the absence of self-propulsion, $\mathbf{V}_n^a = 0$ and self-rotation $\boldsymbol{\Omega}_n^a = 0$. Propulsion matrices, and not mobility matrices, are the key quantities that describe the correlated motion of active particles in a viscous fluid, constrained by the conservation of momentum and angular momentum [24]. While mobility and propulsion matrices have to be computed numerically for particles of general shape, analytical expressions can be derived when the particles are spheres [24].

Here, we use mobility and propulsion matrices for spheres of radius a , computed in the superposition approximation first introduced by Kirkwood and Riseman [25], again, in the context of the dynamics of a polymer. In this approximation, the mobility matrices reduce to the well-known Rotne-Prager-Yamakawa tensors while the propulsion matrices are obtained analytically [24] as gradients of the fundamental solution of the Stokes equation for an unbounded fluid. For a passive polymer, Yoshizaki and Yamakawa [26] verified that the superposition approximation is correct to $\mathcal{O}((a/b)^3)$, where b is the mean separation between spheres, as $N \rightarrow \infty$. Since the propulsion matrices decay more rapidly with separation than mobility matrices, the superposition approximation for active filaments is also accurate to $\mathcal{O}((a/b)^3)$ [24]. The resulting equations of motion are used to study the dynamics of active filaments where the spheres produce dipolar flows and, so, are not individually motile. This part of our work complements studies of active filaments consisting of individually motile particles. We emphasize that our general theory includes both the motile and non-motile cases studied previously.

In the next section we present a generalization of the theory of Brownian motion of hydrodynamically interacting spherical particles to include surface activity. In section III, we construct equations of motion for active filaments using the results of this general theory. In section IV we introduce a minimal model for an active filament by discarding all but leading terms in the filament equations of motion derived previously. Here we also study dynamics of such active filaments when both ends of the filament are free and when one end is tethered and the other end is free. In the first case, for sufficient strength of activity the filament is unstable to transverse perturbations, which results in a sequence of translational, rotational and oscillatory dynamical steady states. In the second case, we find a sequence of rotational and oscillatory dynamical steady states, both of which are limit cycles in the phase space of the dynamical system described by the equations of motion. In section V, linear stability analysis shows that the transition to a dynamic state happens due a simple instability in both cases. This analysis shows that non-local hydrodynamic interactions are essential for the dynamic instability to occur. We conclude with a discussion of the application of our equations of motion to study collective phenomena in suspensions of active filaments [27, 28] and other soft dissipative structures.

II. BROWNIAN MICROHYDRODYNAMICS OF ACTIVE SPHERES

We consider the motion of N spherical active particles of radius a in an incompressible viscous fluid. The center of the n -th sphere is at \mathbf{R}_n and its orientation is specified by the unit vector \mathbf{p}_n . The fluid can exchange both momentum and angular momentum with the particles, of amounts determined by integrals of the momentum flux over the particle boundaries. In addition to this contact contribution, the particles may be acted on by body forces and torques. At low Reynolds numbers inertia, of both the particles and the fluid, can be neglected, which results in an instantaneous balance of surface and body contributions to forces and torques. Newton's laws, therefore, reduce to a pair of constraints on the fluid stress at the surface of every particle,

$$M\dot{\mathbf{V}}_n = \oint \mathbf{n} \cdot \boldsymbol{\sigma} dS_n + \mathbf{F}_n^e = 0, \quad (2a)$$

$$I\dot{\boldsymbol{\Omega}}_n = \oint \mathbf{r} \times \mathbf{n} \cdot \boldsymbol{\sigma} dS_n + \mathbf{T}_n^e = 0. \quad (2b)$$

The fluid stress $\boldsymbol{\sigma} = -p\mathbb{I} + \eta(\nabla\mathbf{v} + \nabla\mathbf{v}^T)$ has both hydrostatic and viscous contributions and is determined from conditions of incompressibility and local momentum conservation

$$\nabla \cdot \mathbf{v} = 0; \quad \nabla \cdot \boldsymbol{\sigma} = 0. \quad (3)$$

where \mathbf{v} is the fluid velocity, p is pressure and η is the viscosity. The solution of this Stokes system provides the

stress, from which the contact contribution of the force and torque on the every particle can be determined. In the absence of inertia and body forces, the conservation of particle momentum requires that the net contact force and the net contact torque on every particle be zero. The solution of the Stokes equation is determined by the boundary conditions on the particle surfaces and at infinity. While activity can be expressed through a variety of boundary conditions on both the fluid velocity and on the fluid stress, we assume here an active slip at the surface of the particle [24]. This encompasses a wide variety of active phenomena, including electrophoresis, diffusio-phoresis [29], self-phoresis due to chemical catalysis [30], and even swimming of microorganisms [31, 32]. We chose the fluid to be at rest at infinity. The boundary conditions, therefore, are

$$\mathbf{v}(\mathbf{R}_n + \boldsymbol{\rho}_n) = \mathbf{V}_n + \boldsymbol{\Omega}_n \times \boldsymbol{\rho}_n + \mathbf{v}^a(\boldsymbol{\rho}_n) \quad (4a)$$

$$|\mathbf{v}| \rightarrow 0, \quad |p| \rightarrow 0, \quad |\mathbf{r}| \rightarrow \infty. \quad (4b)$$

The task of obtaining the solution of the Stokes equation is substantially simplified by recognizing that the three-dimensional partial differential equation can be reduced, instead, to a two-dimensional integral equation over the particle boundaries. The starting point of this development is the integral representation of Stokes flow [33, 34],

$$\begin{aligned} 8\pi\eta v_i(\mathbf{r}) = & - \sum_{m=1}^N \int G_{ij}(\mathbf{r}, \mathbf{r}_m) f_j(\mathbf{r}_m) dS_m \\ & + \eta \sum_{m=1}^N \int K_{jik}(\mathbf{r}, \mathbf{r}_m) n_k v_j(\mathbf{r}_m) dS_m \end{aligned} \quad (5)$$

which provides the solution of Stokes equation in terms of the velocity and the traction, $\mathbf{f} = \mathbf{n} \cdot \boldsymbol{\sigma}$, over the particle boundaries. The kernels in the integral representation are the Green's function \mathbf{G} , the pressure vector \mathbf{p} and the stress tensor, \mathbf{K} .

$$p_i(\mathbf{r}, \mathbf{r}') = -\nabla_i \nabla^2 \rho = \frac{\rho_i}{\rho^3} \quad (6a)$$

$$G_{ij}(\mathbf{r}, \mathbf{r}') = (\nabla^2 \delta_{ij} - \nabla_i \nabla_j) \rho = \frac{\delta_{ij}}{\rho} + \frac{\rho_i \rho_j}{\rho^3}; \quad (6b)$$

$$K_{ijk}(\mathbf{r}, \mathbf{r}') = -\delta_{ik} p_j + \nabla_k G_{ij} + \nabla_i G_{jk}. \quad (6c)$$

In the absence of boundaries, these kernels are translationally invariant and, so, are functions of the separation $\boldsymbol{\rho} = \mathbf{r} - \mathbf{r}'$. The boundary integrals can be evaluated analytically by expanding the boundary fields in complete orthogonal bases [24, 35], which are most conveniently chosen to be the tensorial spherical harmonics, $\mathbf{Y}^{(l)}$

$$\mathbf{Y}_{\alpha_1 \alpha_2 \dots \alpha_l}^{(l)}(\hat{\boldsymbol{\rho}}) = (-1)^{l+1} \rho^{l+1} \nabla_{\alpha_1} \dots \nabla_{\alpha_l} \left(\frac{1}{\rho} \right). \quad (7)$$

In this basis, the surface velocity and traction on each

particle is expanded as [35, 36]

$$\mathbf{f}(\mathbf{R}_m + \boldsymbol{\rho}_m) = \sum_{l=0}^{\infty} \frac{2l+1}{4\pi a^2} \mathbf{F}_m^{(l+1)} \odot \mathbf{Y}^{(l)}(\hat{\boldsymbol{\rho}}_m), \quad (8a)$$

$$\mathbf{v}(\mathbf{R}_m + \boldsymbol{\rho}_m) = \sum_{l=0}^{\infty} \frac{1}{l!(2l-1)!!} \mathbf{V}_m^{(l+1)} \odot \mathbf{Y}^{(l)}(\hat{\boldsymbol{\rho}}_m), \quad (8b)$$

where the orthogonality of the basis functions yields the expansion coefficients as

$$\mathbf{F}_m^{(l+1)} = \frac{1}{l!(2l-1)!!} \int \mathbf{f}(\mathbf{R}_m + \boldsymbol{\rho}_m) \mathbf{Y}^{(l)}(\hat{\boldsymbol{\rho}}_m) dS_m, \quad (9a)$$

$$\mathbf{V}_m^{(l+1)} = \frac{2l+1}{4\pi a^2} \int \mathbf{v}(\mathbf{R}_m + \boldsymbol{\rho}_m) \mathbf{Y}^{(l)}(\hat{\boldsymbol{\rho}}_m) dS_m. \quad (9b)$$

These expansion coefficients are tensors of rank $l+1$, symmetric and irreducible in their last l indices [24, 35]. The forces, torques, velocities and angular velocities are obtained from

$$\mathbf{F}_m^{(1)} = -\mathbf{F}_m^e; \quad 2\epsilon \cdot a \mathbf{F}_m^{(2)} = \mathbf{T}_m^e$$

$$\mathbf{V}_m^{(1)} = \mathbf{V}_m - \langle \mathbf{v}_m^a \rangle; \quad 2\epsilon \cdot \mathbf{V}_m^{(2)} = -a \boldsymbol{\Omega}_m + \frac{3}{2a} \langle \boldsymbol{\rho}_m \times \mathbf{v}_m^a \rangle$$

where the angle brackets indicate integration of the enclosed term over the surface of the sphere and dividing the result by the surface area. Inserting the expansions in the boundary integral representation leads to a succinct expression for the fluid flow in terms of the expansion coefficients [24],

$$\begin{aligned} 8\pi\eta \mathbf{v}(\mathbf{r}) = & - \sum_{m=1}^N \sum_{l=0}^{\infty} \mathbf{G}^{(l+1)}(\mathbf{r}, \mathbf{R}_m) \odot \mathbf{F}_m^{(l+1)} \\ & + \eta \sum_{m=1}^N \sum_{l=1}^{\infty} \mathbf{K}^{(l+1)}(\mathbf{r}, \mathbf{R}_m) \odot \mathbf{V}_m^{(l+1)}. \end{aligned} \quad (10)$$

The boundary integrals $\mathbf{G}^{(l)}$ and $\mathbf{K}^{(l)}$ can be evaluated explicitly in terms of the Green's function \mathbf{G} and its derivatives. In this expression, the velocity coefficients can be computed from the boundary condition, but the traction coefficients remain unknown. To determine the traction coefficients, the boundary condition is first enforced on the boundary of n -th particle, the resulting equation is weighted by the l -th tensorial harmonic and finally integrated over the n -th boundary. This Galerkin procedure yields an infinite-dimensional linear system of equations for the unknown traction coefficients [24],

$$\begin{aligned} 4\pi\eta \mathbf{V}_n^{(l+1)} = & - \sum_{m=1}^N \sum_{l'=0}^{\infty} \mathbf{G}_{nm}^{(l+1, l'+1)}(\mathbf{R}_n, \mathbf{R}_m) \odot \mathbf{F}_m^{(l'+1)} \\ & + \eta \sum_{m=1}^N \sum_{l'=1}^{\infty} \mathbf{K}_{nm}^{(l+1, l'+1)}(\mathbf{R}_n, \mathbf{R}_m) \odot \mathbf{V}_m^{(l'+1)}. \end{aligned} \quad (11)$$

where the matrix elements $\mathbf{G}_{nm}^{(l, l')}$ and $\mathbf{K}_{nm}^{(l, l')}$ can, again, be evaluated analytically in terms of the Green's function

\mathbf{G} and its derivatives [24]. The formal solution of this linear system yields Eq. 1, which expresses the rigid body motion in terms of the body forces and body torques and the coefficients of the active slip velocity. These equations reflect the linearity of both the Stokes equations and the boundary conditions. The hydrodynamically correlated motion is a sum of passive terms, proportional to the external body forces and torques, and active terms, proportional the modes of the active velocity. The last terms in each of the equations are the self-propulsion and self-rotation velocities of an isolated active sphere, which are given in terms of the active slip velocity as

$$4\pi a^2 \mathbf{V}_n^a = - \int \mathbf{v}^a(\boldsymbol{\rho}_n) dS_n \quad (12a)$$

$$4\pi a^2 \boldsymbol{\Omega}_n^a = - \frac{3}{2a^2} \int \boldsymbol{\rho}_n \times \mathbf{v}^a(\boldsymbol{\rho}_n) dS_n \quad (12b)$$

The above two equations have been known in the context of phoresis [37] and swimming by surface distortions [38]. They were later derived by the use of the Lorentz reciprocal relation [39]. The work of [35] derives these from the boundary integral representation of Stokes flow. The propulsion matrices emerge naturally from the solution of the boundary integral equation as coefficients that determine the active contribution to the hydrodynamic interaction. Thus, Eq. 1 expresses hydrodynamic interactions between active particles acted upon by external forces and torques [24].

We note that the boundary integral method yields the hydrodynamic interaction between particles without the need to resolve bulk fluid degrees of freedom. This makes

Eq. 1 especially useful for computing the hydrodynamic interaction of active particles in three dimensions, as the computational cost of resolving fluid degrees of freedom is completely eliminated [24, 40].

The addition of Brownian fluctuations to Eq. 1 is accomplished by appeal to linearity, the balance of dissipation and fluctuation and Onsager symmetry of the mobilities. The generalization of the Einstein-Smoluchowski description of the diffusion of a passive colloidal particle to the hydrodynamically correlated diffusive motion of N colloidal particles was completed by several authors using Liouville, kinetic theory, Fokker-Planck and Langevin approaches [41]. The Langevin approach provides the most direct way of incorporating in Eq. 1 by promoting them to a set of stochastic differential equations with a state-dependent fluctuation. The fluctuations are chosen to compensate each source of dissipation such that distribution of positions and orientations is Gibbsian in the absence of activity. The fluctuations, then, are correlated Wiener processes with variances proportional to the mobility matrices. The positivity of dissipation ensures that mobility matrices are positive-definite and Onsager symmetry constrains them to be symmetric in both the particle and translation-rotation indices. These two properties ensure that a mobility matrix can be factorised into a lower triangular matrix and its transpose, any one of which is a ‘‘square-root’’ of the mobility matrix. The fluctuations can then be expressed as products of uncorrelated Wiener processes $\boldsymbol{\xi}^T, \boldsymbol{\xi}^R, \boldsymbol{\eta}^T, \boldsymbol{\eta}^R$ and the ‘‘square-root’’ Cholesky factors. By linearity, dissipative, Brownian and active motions are additive. Therefore, the generalization of Brownian hydrodynamics to N active particles, expressed as coupled Langevin equations, is

$$\mathbf{V}_n = \underbrace{\sum_{m=1}^N \boldsymbol{\mu}_{nm}^{TT} \cdot \mathbf{F}_m + \boldsymbol{\mu}_{nm}^{TR} \cdot \mathbf{T}_m}_{Passive} + \underbrace{\sum_{m=1}^N \sqrt{2k_B T \boldsymbol{\mu}_{nm}^{TT}} \cdot \boldsymbol{\xi}_m^T + \sqrt{2k_B T \boldsymbol{\mu}_{nm}^{TR}} \cdot \boldsymbol{\xi}_m^R}_{Brownian} + \underbrace{\sum_{m \neq n} \sum_{l=1}^{\infty} \boldsymbol{\pi}_{nm}^{(T, l+1)} \odot \mathbf{V}_m^{(l+1)} + \mathbf{V}_n^a}_{Active} \quad (13a)$$

$$\boldsymbol{\Omega}_n = \underbrace{\sum_{m=1}^N \boldsymbol{\mu}_{nm}^{RT} \cdot \mathbf{F}_m + \boldsymbol{\mu}_{nm}^{RR} \cdot \mathbf{T}_m}_{Passive} + \underbrace{\sum_{m=1}^N \sqrt{2k_B T \boldsymbol{\mu}_{nm}^{RT}} \cdot \boldsymbol{\eta}_m^T + \sqrt{2k_B T \boldsymbol{\mu}_{nm}^{RR}} \cdot \boldsymbol{\eta}_m^R}_{Brownian} + \underbrace{\sum_{m \neq n} \sum_{l=1}^{\infty} \boldsymbol{\pi}_{nm}^{(R, l+1)} \odot \mathbf{V}_m^{(l+1)} + \boldsymbol{\Omega}_n^a}_{Active} \quad (13b)$$

These equations are the main result of this section. In the absence of activity, they reduce to the equation of Brownian dynamics with hydrodynamic interactions [42]. When the forces derive from positional and angular potentials, the form chosen for the fluctuations ensures that the Gibbs distribution of the positions and orientations is the stationary distribution. When activity is included, the balance between fluctuation and dissipation is no longer maintained and stationary states are no longer described by the Gibbs distribution. As we show in the remainder of the paper, non-trivial stationary states are obtained when the spheres are chained together into fil-

aments.

III. BROWNIAN MICROHYDRODYNAMICS OF ACTIVE FILAMENTS

The equations of active Brownian hydrodynamics presented in the previous section form the basis of our theory of active slender bodies. As mentioned before, we approximate the slender body as a filament, and then discretize the filament as a set of connected beads. The forces in the active Brownian hydrodynamic equations

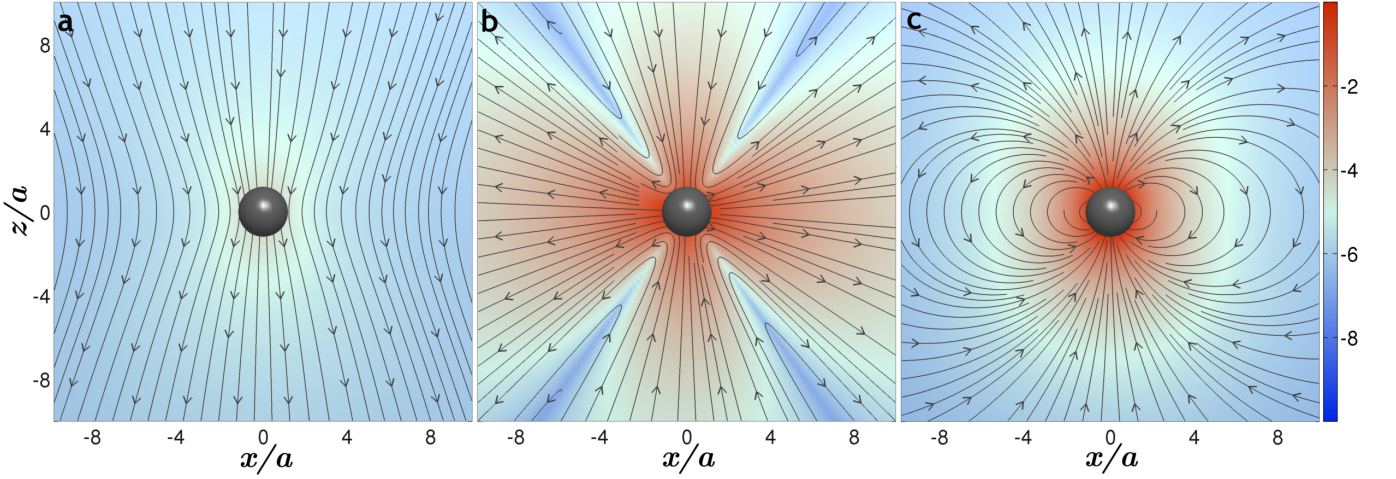


Figure 1. Streamlines of irreducible modes of slow viscous flow around an active sphere. Displayed in (a) is $\mathcal{F}^0 \mathbf{G} \cdot \mathbf{F}$, the flow around a sphere translating under the action of a force \mathbf{F} ; in (b) is $\mathcal{F}^1 \nabla \mathbf{G} \odot \mathbf{V}^{(2)}$, the minimal flow around a non-motile active sphere; and in (c) is $\nabla^2 \mathbf{G} \odot \mathbf{V}^{(3)}$, the minimal flow around a motile active sphere. In the limit $a \rightarrow 0$, the flows in (a) and (b) reduce to a Stokeslet and stresslet, respectively, while (c) is a degenerate velocity quadrupole. The background colour is proportional to the logarithm of the velocity magnitude.

then are derivatives of the non-linear spring potentials,

$$\mathbf{F}_n = -\nabla_n U$$

We assume the potential U to be a sum of connectivity, elastic, and self-avoidance potentials,

$$U = \sum_{m=1}^{N-1} U^C(\mathbf{R}_m, \mathbf{R}_{m+1}) + \sum_{m=2}^{N-1} U^E(\mathbf{R}_{m-1}, \mathbf{R}_m, \mathbf{R}_{m+1}) + \sum_{m < n} U^S(\mathbf{R}_n, \mathbf{R}_m) \quad (14)$$

The connectivity potential $U^C(\mathbf{R}, \mathbf{R}') = k(r - b_0)^2/2$, with elasticity parameter k , penalizes departures of the distance, $r = |\mathbf{R} - \mathbf{R}'|$, of two consecutive particles from the equilibrium value of b_0 . The elastic potential for bending $U^E = \bar{\kappa}(1 - \cos\phi)$, with rigidity parameter $\bar{\kappa}$, penalizes departures of the angle ϕ between consecutive bonds from their equilibrium value of zero. The rigidity parameter $\bar{\kappa}$ connects to bending rigidity κ as $\bar{\kappa} = \kappa b_0$. The self-avoidance potential U^S restricts the overlap of particles and is taken here to be a Lennard-Jones potential that vanishes smoothly at a distance $\sigma_{LJ} = 2^{1/6}\sigma$. The net force on the filament vanishes, as can be easily verified by summing the force on each particle.

An approximate method for computing the hydrodynamic interactions, used widely in the dynamics of polymers, is to neglect their many-body character and, instead, assume them to be pair-wise additive. This superposition approximation, first introduced by Kirkwood and Riseman [25], yields the well-known Rotne-Prager-Yamakawa form for the translational mobility. In that approximation, the mobility matrices of Eq. 1 are,

$$8\pi\eta\mu_{nm}^{TT} = \begin{cases} \frac{4}{3}a^{-1}\delta & m = n \\ \mathcal{F}^0 \mathcal{F}^0 \mathbf{G}(\mathbf{R}_n, \mathbf{R}_m) & m \neq n \end{cases} \quad (15a)$$

$$8\pi\eta\mu_{nm}^{TR} = \begin{cases} 0 & m = n \\ \frac{1}{2} \nabla_m \times \mathbf{G}(\mathbf{R}_n, \mathbf{R}_m) & m \neq n \end{cases} \quad (15b)$$

$$8\pi\eta\mu_{nm}^{RT} = \begin{cases} 0 & m = n \\ \frac{1}{2} \nabla_n \times \mathbf{G}(\mathbf{R}_n, \mathbf{R}_m) & m \neq n \end{cases} \quad (15c)$$

$$8\pi\eta\mu_{nm}^{RR} = \begin{cases} a^{-3}\delta & m = n \\ \frac{1}{4} \nabla_n \times \nabla_m \times \mathbf{G}(\mathbf{R}_n, \mathbf{R}_m) & m \neq n \end{cases} \quad (15d)$$

The diagonal parts of these matrices are one-body terms while the off-diagonal parts represent the hydrodynamic interactions. The diagonal parts are the familiar Stokes translational and rotational mobilities while the off-diagonal parts can be recognised as the Rotne-Prager-Yamakawa tensors and their generalizations to rotational motion. The Onsager symmetry of the mobility matrix is manifest in these expressions. In the same approximation the propulsion matrices are [24]

$$8\pi\eta\pi_{nm}^{(T, l+1)} = \begin{cases} 0 & m = n \\ c_l \mathcal{F}^0 \mathcal{F}^l \nabla_m^{(l)} \mathbf{G}(\mathbf{R}_n, \mathbf{R}_m) & m \neq n \end{cases} \quad (16a)$$

$$8\pi\eta\pi_{nm}^{(R, l+1)} = \begin{cases} 0 & m = n \\ \frac{c_l}{2} \nabla_n \times \nabla_m^{(l)} \mathbf{G}(\mathbf{R}_n, \mathbf{R}_m) & m \neq n \end{cases} \quad (16b)$$

where, \mathcal{F}^l is the operator

$$\mathcal{F}^l = \left(1 + \frac{a^2}{4l+6} \nabla^2\right).$$

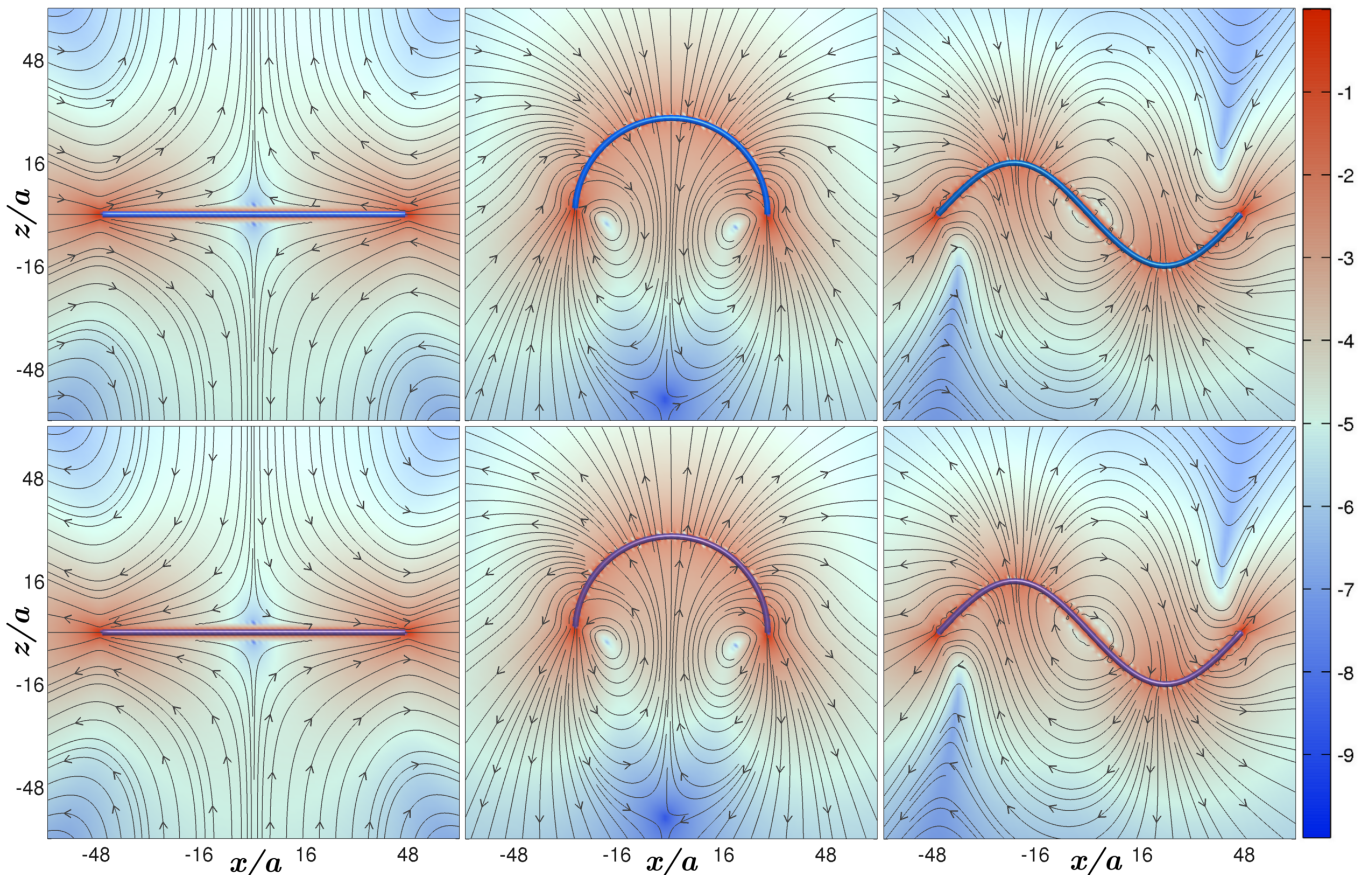


Figure 2. Streamlines of slow viscous flow around contractile (top row) and extensile (bottom row) minimally active filaments. Spontaneous flow in the linear conformation tends to compress contractile filaments and extend extensile filaments (first column). Both symmetric and antisymmetric transverse perturbations are suppressed in contractile filaments but enhanced in extensile filaments by the spontaneous flow (second and third columns). The latter leads to a linear instability in extensile filaments, when the elastic restoring force is no longer sufficient to counter the destabilizing tendency of the spontaneous flow.

that accounts for the finite-size Faxen correction for the flow due to a sphere of radius a and c_l is a numerical constant. The propulsion matrices, as defined here, represent hydrodynamic interactions and, therefore, are purely off-diagonal. The self-propulsion and self-rotation are wholly contained, respectively, in the diagonal terms \mathbf{V}_n^a and $\mathbf{\Omega}_n^a$.

For an active filament, the rotational motion of the spheres can be ignored, assuming torsional potentials

that prevent such rotations. Therefore, the orientation of the spheres is no longer a dynamical degree of freedom to be determined from the angular velocity, but is prescribed. It is natural to fix the orientation of n -th sphere, $\mathbf{p}_n = \alpha \mathbf{t}_n + \beta \mathbf{n}_n + \gamma \mathbf{b}_n$, in the local Frenet-Serret frame in terms of the of the tangent \mathbf{t}_n , normal \mathbf{n}_n and binormal \mathbf{b}_n , and the direction cosines α , β and γ . Combining all of the above, we obtain the following equation of motion for active filaments,

$$\begin{aligned} \dot{\mathbf{R}}_n = & \frac{\mathbf{F}_n}{6\pi\eta a} + \frac{1}{8\pi\eta} \sum_{m \neq n}^N \mathcal{F}^0 \mathcal{F}^0 \mathbf{G}(\mathbf{R}_n, \mathbf{R}_m) \cdot \mathbf{F}_m + \left(\frac{2k_B T}{6\pi\eta a} \right)^{\frac{1}{2}} \boldsymbol{\xi}_n + \sum_{m \neq n}^N \left(\frac{2k_B T \mathcal{F}^0 \mathcal{F}^0 \mathbf{G}(\mathbf{R}_n, \mathbf{R}_m)}{8\pi\eta} \right)^{\frac{1}{2}} \cdot \boldsymbol{\xi}_m \\ & + \frac{1}{8\pi\eta} \sum_{m \neq n}^N \sum_{l=1}^{\infty} \underbrace{c_l \mathcal{F}^0 \mathcal{F}^l \nabla_m^{(l)} \mathbf{G}(\mathbf{R}_n, \mathbf{R}_m) \odot \mathbf{V}_m^{(l+1)}}_{Active} + \mathbf{V}_n^a \end{aligned} \quad (17)$$

These stochastic differential equations describe the Brownian

dynamics of an extensile, semi-flexible, self-

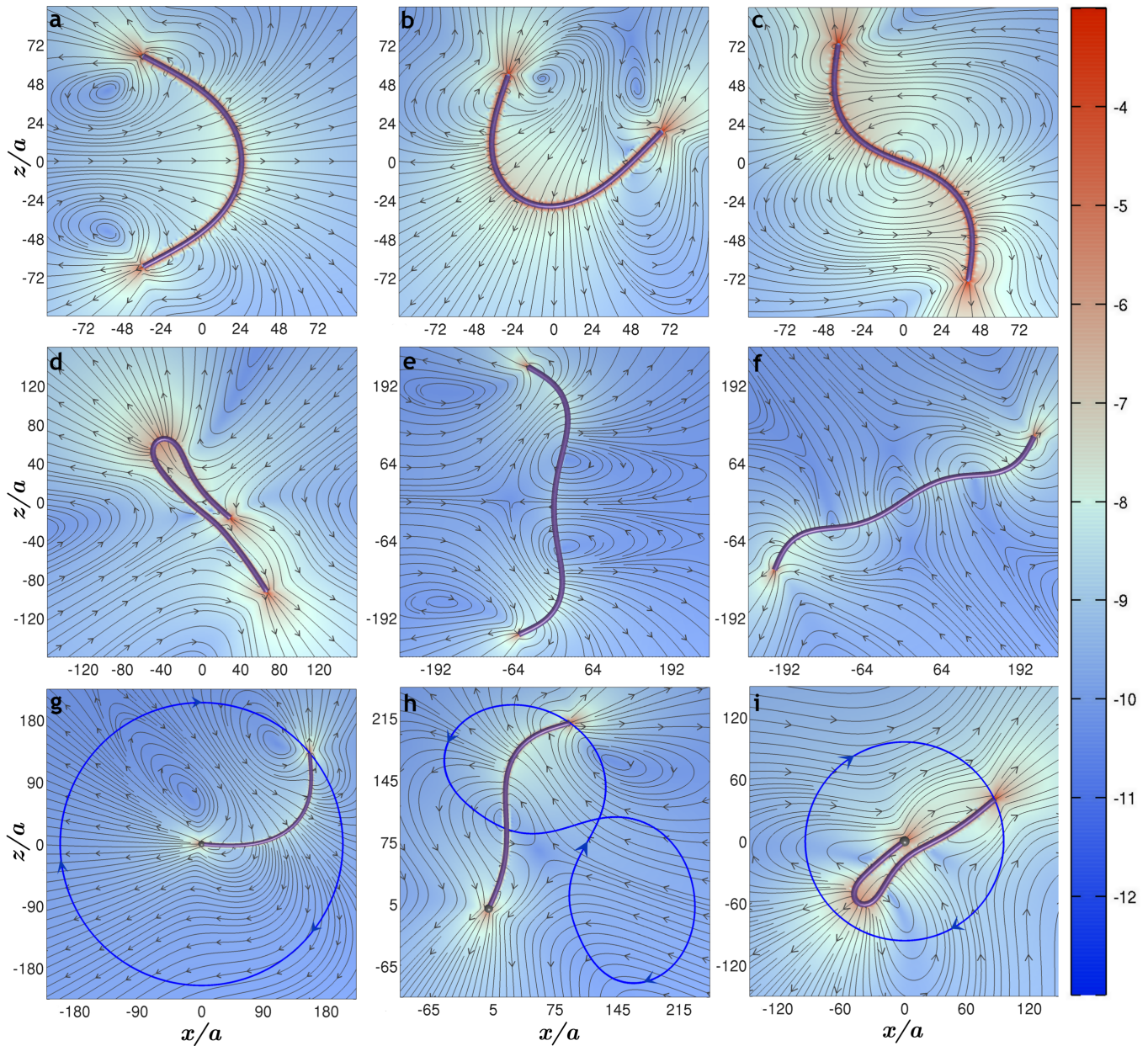


Figure 3. Non-equilibrium stationary states of a free, (a) - (f), and tethered, (g) - (i), minimally active filament. The figures show the filament conformation and the streamlines of slow viscous flow produced by the activity, where the background is coloured by the logarithm of the magnitude of the velocity. Free filament steady states are shown for three lengths with increasing values of activity \mathcal{A}_s . For short filaments ($N = 48$) increasing activity produces the three non-equilibrium steady states in (a) - (c), corresponding to the excitation of the first two elastic eigenmodes and their linear combinations. As the filament length is increased ($N = 80$ and $N = 128$) higher elastic eigenmodes appear with increasing amounts of activity in (d) - (f). Tethered filament steady states are shown for a fixed length ($N = 64$). Increasing activity produces a rotating steady state in (g), which bifurcates into an oscillating steady state in (h), with a return to a distinct rotating steady state in (i). (Movie)

avoiding active filament including hydrodynamic interactions that arise from the exchange of momentum between the filament and its local conservation in the bulk fluid. These equations are the natural extension of Brownian hydrodynamics of passive filaments to the active case. In the next section, we study the simplest version of these

equations, where only the most dominant contribution to active flow is retained and Brownian fluctuations are neglected.

IV. DYNAMICS OF MINIMALLY ACTIVE FILAMENTS

In this section, we study in detail the simplest member of the family of models described by the general equations of motion (Eq. 17) of the previous section. In this minimal model, the spheres are non-motile, $\mathbf{V}_n^a = 0$, and all active velocity components other than the symmetric part of $\mathbf{V}_n^{(2)}$ are zero. Thus each individual sphere produces the flow show in Fig. 1b. The velocities and tractions are, therefore,

$$\mathbf{v}(\mathbf{R}_m + \boldsymbol{\rho}_m) = \dot{\mathbf{R}}_m + \mathbf{s}_m \cdot \boldsymbol{\rho}_m \quad (18a)$$

$$4\pi a^2 \mathbf{f}(\mathbf{R}_m + \boldsymbol{\rho}_m) = -\nabla_m U + 3\mathbf{S}_m \cdot \boldsymbol{\rho}_m \quad (18b)$$

where \mathbf{s}_m and \mathbf{S}_m are, respectively, the symmetric parts of the second-rank velocity and traction coefficients. The solution of the boundary integral equation, in the diagonal approximation, relates the unknown traction coefficient to the known value of the velocity coefficient [24, 35]

$$\mathbf{S}_m = -\frac{3}{20\pi\eta a^3} \mathbf{s}_m \quad (19)$$

To complete the model, it is necessary to specify the orientation \mathbf{p}_n of the spheres, and hence the principal axis of the stresslet, in relation to the filament conformation. Motivated by the experimental observation that molecular motors walking on microtubules generate tangential stresses [1], we parametrize \mathbf{s}_m uniaxially, with its principal axis always parallel to the local tangent \mathbf{t}_m of the filament,

$$\mathbf{s}_m = s_0(\mathbf{t}_m \mathbf{t}_m - \frac{1}{3}\boldsymbol{\delta}). \quad (20)$$

The coefficient s_0 is positive for extensile stresses and negative for contractile stresses. Additionally, we assume that the activity is so large that the Brownian fluctuations make a negligible contribution to the dynamics. Active flow is balanced entirely by the filament elasticity. This leads to deterministic equations of motion for an active filament composed of non-motile beads,

$$\begin{aligned} \dot{\mathbf{R}}_n = & -\frac{1}{6\pi\eta a} \nabla_n U - \frac{1}{8\pi\eta} \sum_{m \neq n} \mathcal{F}^0 \mathcal{F}^0 \mathbf{G} \cdot \nabla_m U \\ & + \frac{7a^3}{6} \sum_{m \neq n} \underbrace{\mathcal{F}^0 \mathcal{F}^1 \nabla \mathbf{G} \odot \mathbf{s}_m}_{Active}. \end{aligned} \quad (21)$$

These equations, without finite-sized corrections to the hydrodynamic flow, were first proposed in [19] and subsequently used in [20] to study the dynamics of clamped active filaments.

The flow produced by the filament is sum of contributions from the potentials and the activity,

$$\mathbf{v}(\mathbf{r}) = -\frac{1}{8\pi\eta} \sum_{n=1}^N \mathcal{F}^0 \mathbf{G} \cdot \nabla_n U + \frac{7a^3}{6} \sum_{n=1}^N \underbrace{\mathcal{F}^1 \nabla \mathbf{G} \odot \mathbf{s}_n}_{Active}. \quad (22)$$

The resultant flow is shown for three conformations, for both extensile and contractile filaments, in Fig 2. In the linear conformation, shown in the first column of Fig 2, the flow tends to compress contractile filaments and extend extensile filaments. The stationary length of the filament, then, is somewhat shorter in the contractile flow but somewhat longer in the extensile flow. In a symmetrically curved conformation, shown in the second column of Fig, 2, the spontaneous flow tends to suppress curvature in the contractile filaments but tends to enhance it for extensile filaments. The suppression and enhancement is seen for antisymmetrically curved conformations in the third row of Fig. 2. This shows that the interplay of flow and curvature is generally stabilizing for contractile filaments while it is destabilizing for extensile filaments. On dimensional grounds, a linear instability is expected when the filament length $L > l_A \sim \kappa/s_0$. In the remainder of the paper, we shall focus only on extensile filaments and study the non-equilibrium stationary states that appear as a consequence of the linear instability.

In d spatial dimensions, activity introduces a new rate $\Gamma_s = s_0/\eta L^d$ in addition to the rate of elastic relaxation $\Gamma_\kappa = \kappa/\eta L^{d+1}$ of the filament bending modes. The ratio, $\mathcal{A}_s = L s_0/\kappa$, of these two time scales provides a dimensionless measure of activity. The activity number \mathcal{A}_s also measures the departure from equilibrium and the amount of energy is injected into the fluid by the filament. We vary both the filament length and the activity number in studying the dynamics of the filament in $d = 3$ dimensions.

We integrate the equations of filament equations of motion numerically using a variable coefficient method. We chose the following parameters for the model : spring constant $k = 1$, bondlength $b_0 = 4a$, rigidity parameter $\bar{\kappa} = 0.4$, stresslet strength $s_0 = 0.0 - 0.5$ and number of spheres $N = 32 - 128$. We obtain the mobility and propulsion matrices using the PyStokes library [40]. We simulate the system for several hundred active relaxation time scales with an initial condition that is linear with small random, transverse perturbations. We study two cases, the first in which the filament is free at both ends and second in which it is free at one end and tethered at the other end.

Our results are summarised in Fig. 3, which shows the non-equilibrium stationary states for both free filaments in panels (a) - (f) and for tethered filaments in panels (g) - (i). A linear instability appears at $\mathcal{A}_s \sim 12$ in free filaments which leads to spontaneous symmetric curvature and an emergent autonomous motility, shown in panel (a). The conformation corresponds, roughly, to the first elastic eigenmode of the passive filament. With increasing amounts of activity, higher elastic eigenmodes appear through a series of bifurcations, shown in panels (b) - (f). Whenever the conformation is asymmetrical about the center, the filament acquires a rotational component of motion. The higher elastic eigenmodes appear for smaller values of activity in longer filament, as is seen by comparing panel (c) with panels (e) and (f). Although the

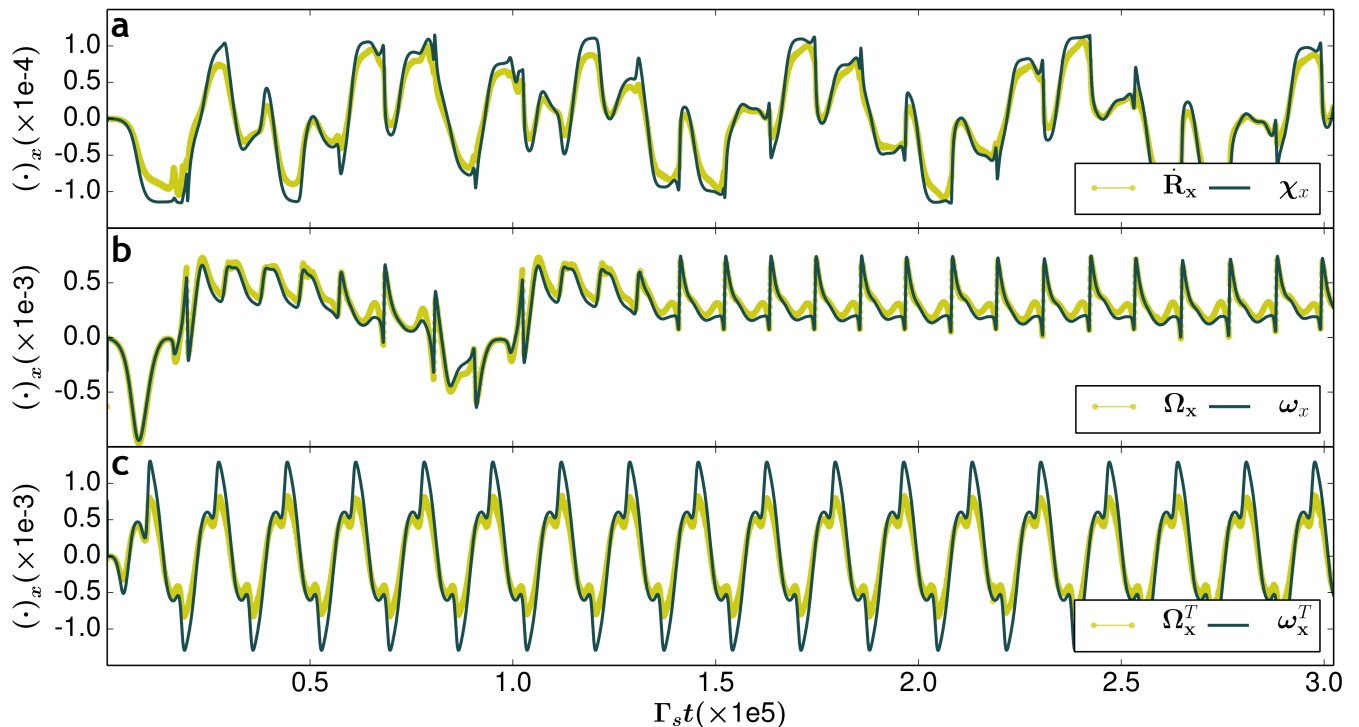


Figure 4. Comparison of filament kinematics and curvature dynamics. In (a) the x -component of the center of mass velocity is compared with the x -component of the scaled average curvature vector (see Eq. 23) for a free filament. In (b) the x -component of the mean angular velocity about the center of mass is compared with the scaled average first moment of the curvature vector (see Eq. 24). In (c) the same comparison is made for a tethered filament, with origin at the point of pivot. The comparison shows that the filament motion is strongly correlated with dynamics of activity induced curvature.

system is three-dimensional, filament motion is planarly stable, in a plane that is determined by the initial condition. This rich dynamics (movie I) and non-equilibrium steady states we have found is remarkably similar to an experiment on an isolated axoneme [9].

Tethering the filament at one end, restricts translation and thus the energy transduction from the activity is fed into rotational and oscillatory states (Movie II). Beyond the threshold activity of $\mathcal{A}_s \sim 5$, a tethered filament rotates around the pivot, panel (g), in a plane that is chosen by the initial condition. Further energy injection leads to flagella like beating in a plane, shown in panel (h). The highest value of activity studied is shown in panel (i), where a conformation similar to panel (d) appears, but now constrained by the pivot, is forced to rotate while maintaining conformation. With increase in filament length and activity, we expect higher elastic eigenmodes to appear, and either rotate or oscillate under the constraint of the tether.

The dynamics of the center of mass follows from summing the equation of motion over all spheres. The contribution from internal spring forces vanishes, and on approximating the active flow by its contribution from the nearest neighbours, an approximate equation is obtained that relates the center of mass motion to the filament

curvature and the activity,

$$\mathbf{V}_{CM} \simeq -\frac{s_0}{4\pi\eta b_0} \langle \lambda \hat{\mathbf{n}} \rangle = \boldsymbol{\chi} \quad (23)$$

In Fig. 4a, we compare the numerically computed values of the center of mass velocity with the curvature vector $\boldsymbol{\chi}$ defined above. There is a surprisingly good agreement between the two, indicating that principal effect of the non-local active flow can be expressed locally as a tendency to promote curvature. A similar relation holds for the angular velocity about the center of mass,

$$\boldsymbol{\Omega}_{CM} \simeq -\frac{s_0}{8\pi\eta b_0} \langle \lambda \hat{\mathbf{n}} \times (\mathbf{R} - \mathbf{R}_{CM}) \rangle = \boldsymbol{\omega} \quad (24)$$

and the previous comparison is repeated for both free and tethered filaments in Fig 4b and Fig 4c. For tethered filaments the pivot point, and not the center of mass, is used to compute cross products, and the activity-dependent prefactor is two times smaller. This suggests that effective, local equations of motion may be accurate for describing some aspects of the dynamics of active filaments.

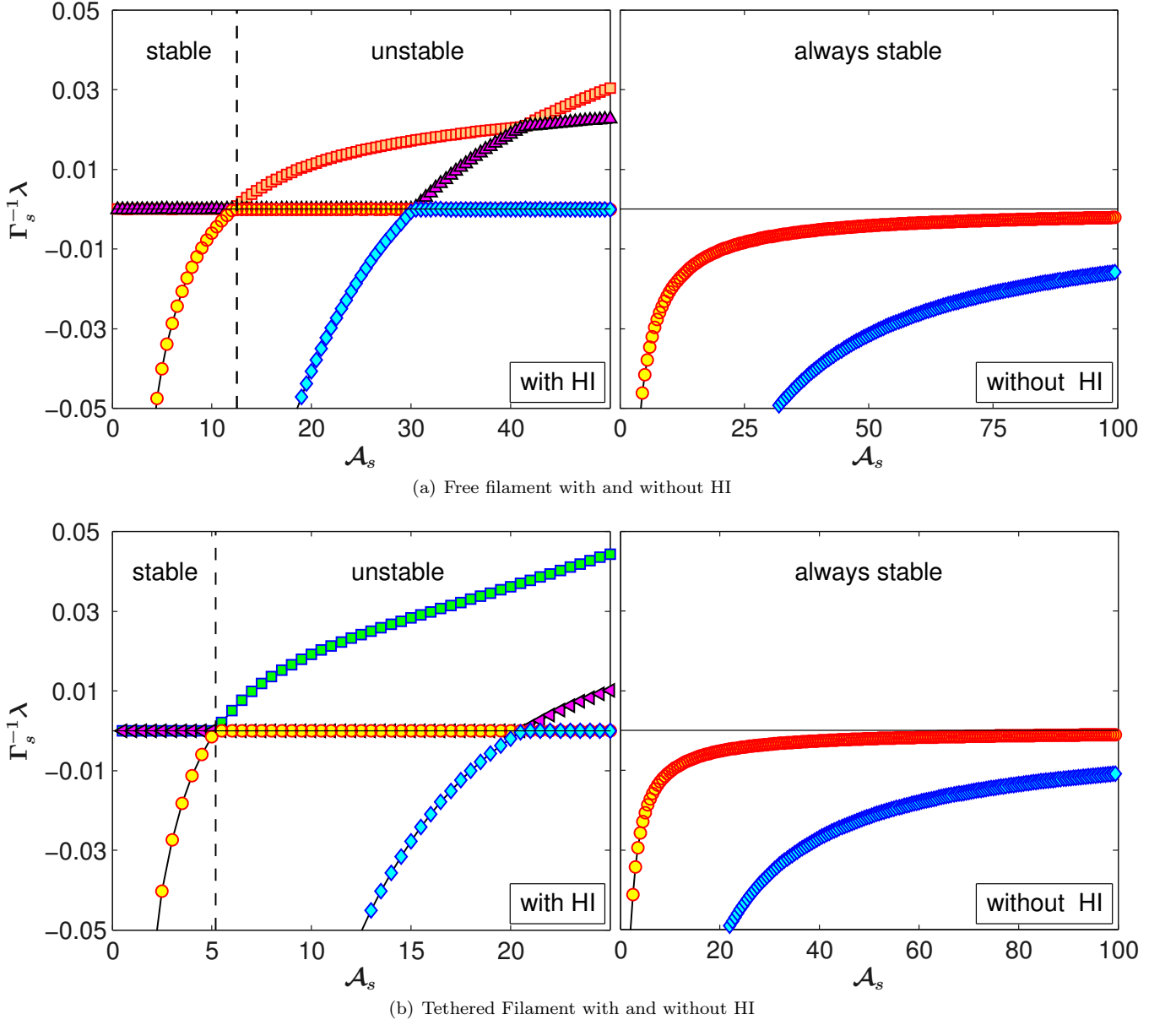


Figure 5. Variation of the largest non-zero eigenvalues of the stability matrix, \mathbf{J} , plotted against activity number, \mathcal{A}_s , for a free filament in (a) and a tethered filament in (b). In each case, the eigenvalues are computed including full hydrodynamic interactions (HI) (left panels) and neglecting all non-local hydrodynamic contributions (right panels). The eigenvalues remain negative, for all values of \mathcal{A}_s in a large range, when hydrodynamic interactions are neglected. Hydrodynamic interactions, therefore, are essential for the instability of the linear conformation and the bifurcation to dynamical steady states, signalled by the positive eigenvalues in each of the left panels.

V. LINEAR STABILITY ANALYSIS

To better understand the linear instability which is expected from the flows shown in Fig 2, we perform a stability analysis of the equations of motion, about the linear conformation. Taking the equations of motion to represent a dynamical system, $\dot{\mathbf{R}}_n = f(\mathbf{R}_1, \mathbf{R}_2, \dots, \mathbf{R}_n)$, we compute the Jacobian $\mathbf{J} = -\nabla_n f|_{\mathbf{R}_n^0}$ at the stationary state with linear conformation \mathbf{R}_n^0 . The linearised

dynamics, then, is

$$\delta\dot{\mathbf{R}}_n = \mathbf{J} \cdot \delta\mathbf{R}_n \quad (25)$$

We numerically compute the eigenvalues of this stability matrix as a function of activity \mathcal{A}_s for both free and tethered filaments. To evaluate the importance of non-local hydrodynamic interactions, we also compare the eigenvalues for the dynamics in which all non-local (that is $m \neq n$) terms are deleted. The results are shown in Fig. 5(a) and Fig. 5(b) for free and tethered filaments,

respectively.

We see that the largest eigenvalue becomes positive at $\mathcal{A}_s \sim 12$ for free filaments and $\mathcal{A}_s \sim 5$ for tethered filaments. The bifurcation is thus a simple instability and not of the Hopf type reported in the previous study of a clamped minimally active filament [20]. The first eigenmode instability flows to the symmetrically curved conformation shown in Fig 3 (a). Instabilities of the higher eigenmodes leads, the first of which is visible in Fig. 5a at $\mathcal{A}_s \sim 40$, produces the more complicated states shown in panels (b) - (g) of Fig 5. The presence of the tether increases the threshold value of the activity at which the instability occurs to $\mathcal{A}_s \sim 5$, but the sequence of instabilities remains identical. Remarkably, there is no instability, in the same range of activity, when hydrodynamic interactions are ignored, as shown in the right panels of Fig 5. Thus, non-local active hydrodynamic flow is essential to produce the instabilities and the non-equilibrium stationary states reported above.

Subsequent bifurcations with increasing values of activity are expected to have a more complicated character, as the stationary states are typically limit cycles. The numerical study of limit cycle instabilities is considerably more involved than that of time-independent stationary states. We shall explore this aspect of the dynamics of active filaments in a future study.

VI. DISCUSSION AND CONCLUSION

Previous work on bead-spring models of active filaments have focused on three distinct mechanisms of activity. In the earliest work of Jayaraman et al [19], activity arises from the hydrodynamic flow of the active spheres. In that work, the equations of motion for filament dynamics in three dimensions contained contributions from the leading order hydrodynamic flow due to stresslets and degenerate quadrupoles. A detailed study and all results were given for non-motile active spheres, thus ignoring the velocity quadrupoles. In subsequent work, Chellakot et al [21] studied a chain of motile active spheres, subject to Brownian motion, in two dimensions but ignored the all non-local hydrodynamic effects, both passive and active. In related work, Jiang and Hou [22] studied a chain of passive spheres, subject to forces of non-equilibrium origin, directed along the filament tangent. In their model, both passive hydrodynamic flow and hydrodynamically correlated Brownian motion is included in three dimensions, but active flow is absent. Remarkably, in spite of these differences between the models, they yield a broadly similar phenomenology : linear instabilities, spontaneous motion, and oscillatory states.

To understand why this might be, it is best to situate all the previous models within the equations of motion presented here. The model studied in detail by Jayaraman et al [19] is obtained when self-propulsion velocities, \mathbf{V}_n^a , are set to zero, only the dipolar contribution to active flow is retained, and finite-sized corrections to

hydrodynamic flow as well as Brownian motion are neglected. The model of Chellakot et al [21] is obtained when the self-propulsion velocity is directed along the axis \mathbf{p}_n , $\mathbf{V}_n^a = v_s \mathbf{p}_n$, and this axis is itself determined from the balance of a restoring and Brownian torques. This requires the angular velocity to be retained as a dynamical variable and all off-diagonal contributions to mobility and propulsion matrices to be ignored. Finally, the model of Jiang and Hou [22] is obtained by ignoring all active components of flow, $\mathbf{v}^a = 0$, but representing the force on the spheres as $\mathbf{F}_n = -\nabla_n U + \alpha \mathbf{t}_n$, as sum of contributions from the potentials and an unspecified non-equilibrium source. The common feature of all these models is that they produce motion in the direction of the curvature. This arises from the non-local hydrodynamic flow in the model of Jayaraman et al, and from the local contributions due to self-propulsion and non-equilibrium activity in the models of Chellakot et al and Jiang et al respectively. The present work shows that a phenomenology beyond curvature instabilities remains to be explored. In particular, torsional instabilities, possible with self-rotating active spheres that are unhindered by torsional potentials, are likely to yield further surprises in the dynamics of active filaments.

The equations of motion presented provide the foundation for studying non-equilibrium statistical mechanics of active filaments. The coupled Langevin equation for the positions can be recast as Fokker-Planck equations, whose stationary solutions in the absence of activity are given by the Gibbs distribution. Activity, in the forms envisaged in this work, introduces an additional drift in the Fokker-Planck equation, destroying the balance between fluctuation and dissipation. This will lead to non-Gibbsian distributions in the stationary state, and, likely change well-known equilibrium properties like statics of the coil-globule transition [43] and the distribution of loop closure times [30]. We urge that some of these problems be addressed both experimentally and through theory and simulations.

As a final remark, we draw attention to the similarity between the instabilities reported here and the convective instability by active stress studied in the pioneering work of Finlayson and Scriven [44].

ACKNOWLEDGMENTS

RA wishes to thank D. Frenkel, M. E. Cates, P. Chaikin, G. Date, A. Donev, S. Ghose, A. J. C. Ladd, I. Pagonabarraga, R. Singh, R. Singh, D. J. Pine, M. J. Shelley, H. A. Stone and P. B. Sunil Kumar for many useful discussions while this work was being completed. RA acknowledges the Hamied Trust for supporting a visit to Cambridge University and the IUSSTF for supporting visits to Princeton University and NYU and warmly thanks D. Frenkel, H. A. Stone and D. J. Pine and for hosting at the respective universities. The authors gratefully acknowledge the Department of Atomic Energy,

Government of India for supporting their research.

Appendix A: Integrals and Matrix elements

The expressions for the boundary integrals $\mathbf{G}^{(l)}$ and $\mathbf{K}^{(l)}$ and the matrix elements $\mathbf{G}_{nm}^{(l,l')}$ and $\mathbf{K}_{nm}^{(l,l')}$ are given as [24],

$$\mathbf{G}^{(l+1)}(\mathbf{r}, \mathbf{R}_m) = \frac{2l+1}{4\pi a^2} \int \mathbf{G}(\mathbf{r}, \mathbf{R}_m + \boldsymbol{\rho}_m) \mathbf{Y}^{(l)}(\hat{\boldsymbol{\rho}}_m) dS_m = a^l \boldsymbol{\Delta}^{(l)} \mathcal{F}^l \nabla_m^{(l)} \mathbf{G}(\mathbf{r}, \mathbf{R}_m) \quad (\text{A1a})$$

$$\mathbf{K}^{(l+1)}(\mathbf{r}, \mathbf{R}_m) = \frac{1}{l!(2l-1)!!} \int \mathbf{K}(\mathbf{r}, \mathbf{R}_m + \boldsymbol{\rho}_m) \cdot \mathbf{n} \mathbf{Y}^{(l)}(\hat{\boldsymbol{\rho}}_m) dS_m = \frac{4\pi a^l \boldsymbol{\Delta}^{(l)}}{(l-1)!(2l+1)!!} \mathcal{F}^l \nabla_m^{(l-1)} \mathbf{K}(\mathbf{r}, \mathbf{R}_m) \quad (\text{A1b})$$

$$\mathbf{G}_{nm}^{(l+1,l'+1)}(\mathbf{R}_n, \mathbf{R}_m) = \begin{cases} \delta_{ll'} \frac{2l+1}{2\pi a} \int \mathbf{Y}^{(l)}(\hat{\boldsymbol{\rho}}) (\boldsymbol{\delta} - \hat{\boldsymbol{\rho}} \hat{\boldsymbol{\rho}}) \mathbf{Y}^{(l)}(\hat{\boldsymbol{\rho}}) d\Omega; & m = n; \\ a^{l+l'} \mathcal{F}_n^l \mathcal{F}_m^{l'} \nabla_n^{(l)} \nabla_m^{(l')} \mathbf{G}(\mathbf{R}_n, \mathbf{R}_m); & m \neq n; \end{cases} \quad (\text{A2a})$$

$$\mathbf{K}_{nm}^{(l+1,l'+1)}(\mathbf{R}_n, \mathbf{R}_m) = \begin{cases} -\delta_{ll'} 4\pi \boldsymbol{\delta} \boldsymbol{\Delta}^{(l)}; & m = n; \\ \frac{4\pi a^{(l+l'+1)}}{(l'-1)!(2l'+1)!!} \mathcal{F}_n^l \mathcal{F}_m^{l'} \nabla_n^{(l)} \nabla_m^{(l'-1)} \mathbf{K}(\mathbf{R}_n, \mathbf{R}_m); & m \neq n; \end{cases} \quad (\text{A2b})$$

Appendix B: Constraining Force on the tethered bead

Tethering the filament generates a conformation dependent constraint force at the tethered point. We take care of hydrodynamics to satisfy the boundary condition appropriately, such that net velocity of the respective end vanishes. Then we back-calculate the constrained force self-consistently on the course of simulation.

$$\dot{\mathbf{R}}_1 = -\frac{1}{6\pi\eta a} (\nabla_1 U + \mathbf{F}_c) - \frac{1}{8\pi\eta} \sum_{m=2}^N \mathcal{F}^0 \mathcal{F}^0 \mathbf{G}(\mathbf{R}_1, \mathbf{R}_m) \cdot \nabla_m U + \frac{7a^3}{6} \sum_{m=2}^N \mathcal{F}^0 \mathcal{F}^1 \nabla \mathbf{G}(\mathbf{R}_1, \mathbf{R}_m) \odot \mathbf{s}_m$$

$$\mathbf{F}_c = -\nabla_1 U - \frac{3}{4\eta} \sum_{m=2}^N \mathcal{F}^0 \mathcal{F}^0 \mathbf{G}(\mathbf{R}_1, \mathbf{R}_m) \cdot \nabla_m U + 7\pi\eta a^4 \sum_{m=2}^N \mathcal{F}^0 \mathcal{F}^1 \nabla \mathbf{G}(\mathbf{R}_1, \mathbf{R}_m) \odot \mathbf{s}_m.$$

-
- [1] Timothy Sanchez, David Welch, Daniela Nicastro, and Zvonimir Dogic. Cilia-Like Beating of Active Microtubule Bundles. *Science*, 333(6041):456, 2011.
 - [2] T. Sanchez, D.T.N. Chen, S.J. DeCamp, M. Heymann, and Z. Dogic. Spontaneous motion in hierarchically assembled active matter. *Nature*, 491:431–434, 2012.
 - [3] H. C. Berg. Motile behavior of bacteria. *Phys. Today*, 53(1):24–30, 2000.
 - [4] S. Ishiwata, N. Okamura, H. Shimizu, T. Anazawa, K. Yasuda, et al. Spontaneous oscillatory contraction (SPOC) of sarcomeres in skeletal muscle. *Advances in biophysics*, 27:227, 1991.
 - [5] C. B. Lindemann and R. Rikmenspoel. Sperm Flagella: Autonomous Oscillations of the Contractile System. *Science*, 175(4019):337–338, 1972.
 - [6] K. E. Machin. Wave propagation along flagella. *J. Exp. Biol.*, 35(May):796–806, 1958.
 - [7] Sébastien Camalet, Frank Jülicher, and Jacques Prost. Self-organized beating and swimming of internally driven filaments. *Phys. Rev. Lett.*, 82(7):1590–1593, 1999.
 - [8] Sébastien Camalet and Frank Jülicher. Generic aspects of axonemal beating. *New J. Phys.*, 2:24–24, October 2000.
 - [9] Matthew Bessen, Rose B Fay, and George B Witman.

- Calcium control of waveform in isolated flagellar axonemes of chlamydomonas. *The Journal of Cell Biology*, 86(2):446–455, 1980.
- [10] F. J. Nédélec, T. Surrey, A. C. Maggs, and S. Leibler. Self-organization of microtubules and motors. *Nature*, 389(6648):305–308, 1997.
- [11] S. Camazine, J. L. Deneubourg, N. R. Franks, J. Sneyd, G. Theraulaz, and E. Bonabeau. *Self-organization in Biological Systems*. Princeton University Press, New York, 2003.
- [12] K Kruse, JF Joanny, F Jülicher, J Prost, and K Sekimoto. Asters, vortices, and rotating spirals in active gels of polar filaments. *Phys. Rev. Lett.*, 92(7):078101, 2004.
- [13] Douglas R Brumley, Kirsty Y Wan, Marco Polin, and Raymond E Goldstein. Flagellar synchronization through direct hydrodynamic interactions. *Elife*, 3:e02750, 2014.
- [14] Douglas R Brumley, Marco Polin, Timothy J Pedley, and Raymond E Goldstein. Hydrodynamic synchronization and metachronal waves on the surface of the colonial alga volvox carteri. *Physical review letters*, 109(26):268102, 2012.
- [15] Wei Wang, Wentao Duan, Ayusman Sen, and Thomas E Mallouk. Catalytically powered dynamic assembly of rod-shaped nanomotors and passive tracer particles. *Proc. Nat. Acad. Sci.*, 110(44):17744–17749, 2013.
- [16] Walter F. Paxton, Kevin C. Kistler, Christine C. Olmeda, Ayusman Sen, Sarah K. St. Angelo, Yanyan Cao, Thomas E. Mallouk, Paul E. Lammert, and Vincent H. Crespi. Catalytic nanomotors: Autonomous movement of striped nanorods. *J. Am. Chem. Soc.*, 126(41):13424–13431, 2004.
- [17] Javier Vicario, Rienk Eelkema, Wesley R. Browne, Auke Meetsma, René M. La Crois, and Ben L. Feringa. Catalytic molecular motors: fuelling autonomous movement by a surface bound synthetic manganese catalase. *Chem. Commun.*, 31:3936–3938, 2005.
- [18] Brian J Williams, Sandeep V Anand, Jagannathan Rajagopalan, and M Taher A Saif. A self-propelled biohybrid swimmer at low reynolds number. *Nature communications*, 5, 2014.
- [19] G. Jayaraman, S. Ramachandran, S. Ghose, A. Laskar, M. Saad Bhamla, P. B. Sunil Kumar, and R. Adhikari. Autonomous Motility of Active Filaments due to Spontaneous Flow-Symmetry Breaking. *Phys. Rev. Lett.*, 109(15):158302, 2012.
- [20] Abhrajit Laskar, Rajeev Singh, Somdeb Ghose, Gayathri Jayaraman, PB Sunil Kumar, and R Adhikari. Hydrodynamic instabilities provide a generic route to spontaneous biomimetic oscillations in chemomechanically active filaments. *Scientific reports*, 3, 2013.
- [21] Raghunath Chelakkot, Arvind Gopinath, L Mahadevan, and Michael F Hagan. Flagellar dynamics of a connected chain of active, polar, Brownian particles. *Journal of The Royal Society Interface*, 11(92):20130884, 2014.
- [22] Huijun Jiang and Zhonghuai Hou. Hydrodynamic interaction induced spontaneous rotation of coupled active filaments. *Soft matter*, 10(46):9248–9253, 2014.
- [23] Huijun Jiang and Zhonghuai Hou. Motion transition of active filaments: rotation without hydrodynamic interactions. *Soft Matter*, 10(7):1012–1017, 2014.
- [24] Rajesh Singh, Somdeb Ghose, and R Adhikari. Many-body microhydrodynamics of colloidal particles with active boundary layers. *Journal of Statistical Mechanics: Theory and Experiment*, 2015(6):P06017, 2015.
- [25] John G Kirkwood and Jacob Riseman. The intrinsic viscosities and diffusion constants of flexible macromolecules in solution. *The Journal of Chemical Physics*, 16(6):565–573, 1948.
- [26] Takenao Yoshizaki and Hiromi Yamakawa. Validity of the superposition approximation in an application of the modified osen tensor to rigid polymers. *The Journal of Chemical Physics*, 73(1):578–582, 1980.
- [27] Ankita Pandey, PB Kumar, and R Adhikari. Flow-induced nonequilibrium self-assembly in suspensions of stiff, apolar, active filaments. *arXiv preprint arXiv:1408.0433*, 2014.
- [28] David Santillan and Michael J. Shelley. Active suspensions and their nonlinear models. *Comptes. Rendus Phys.*, 2013.
- [29] J.L. Anderson and D.C. Prieve. Diffusiophoresis caused by gradients of strongly adsorbing solutes. *Langmuir*, 7(2):403–406, 1991.
- [30] Debarati Sarkar, Snigdha Thakur, Yu-Guo Tao, and Raymond Kapral. Ring closure dynamics for a chemically active polymer. *Soft Matter*, 10:9577–9584, 2014.
- [31] JR Blake. A spherical envelope approach to ciliary propulsion. *J. Fluid Mech.*, 46(1):199–208, 1971.
- [32] Takuji Ishikawa, M. P. Simmonds, and T. J. Pedley. Hydrodynamic interaction of two swimming model microorganisms. *J. Fluid Mech.*, 568(1):119–160, 2006.
- [33] O.A. Ladyzhenskaia. *The mathematical theory of viscous incompressible flow*. Mathematics and its applications. Gordon and Breach, 1969.
- [34] C. Pozrikidis. *Boundary Integral and Singularity Methods for Linearized Viscous Flow*. Cambridge University Press, Cambridge, 1992.
- [35] Somdeb Ghose and R Adhikari. Irreducible representations of oscillatory and swirling flows in active soft matter. *Phys. Rev. Lett.*, 112(11):118102, 2014.
- [36] Anthony JC Ladd. Hydrodynamic interactions in a suspension of spherical particles. *J. Chem. Phys.*, 88:5051, 1988.
- [37] J L Anderson. Colloid transport by interfacial forces. *Annual Review of Fluid Mechanics*, 21(1):61–99, 1989.
- [38] BU Felderhof. Stokesian swimmers and active particles. *arXiv preprint arXiv:1502.00242*, 2015.
- [39] Howard A. Stone and Aravinthan D. T. Samuel. Propulsion of microorganisms by surface distortions. *Phys. Rev. Lett.*, 77:4102–4104, Nov 1996.
- [40] Rajesh Singh, Abhrajit Laskar, and R. Adhikari. Pystokes: Hampi, 2014.
- [41] T. J. Murphy and J. L. Aguirre. Brownian motion of n interacting particles. I. extension of the Einstein diffusion relation to the n particle case. *The Journal of Chemical Physics*, 57(5):2098–2104, 1972.
- [42] Donald L Ermak and JA McCammon. Brownian dynamics with hydrodynamic interactions. *The Journal of chemical physics*, 69(4):1352–1360, 1978.
- [43] Andreas Kaiser, Sonja Babel, Borge ten Hagen, Christian von Ferber, and Hartmut Löwen. How does a flexible chain of active particles swell? *The Journal of chemical physics*, 142(12):124905, 2015.
- [44] BA Finlayson and LE Scriven. Convective instability by active stress. *Proc. Roy. Soc. A*, 310(1501):183–219, 1969.